How well does the virial temperature trace atomic cooling? Gas temperatures and inflow rates in pristine high-redshift haloes

Matthew T. Scoggins,[1★] James Sullivan,[1] Katia Rosario,[3] Jack Nicolaas Van Schaik,[3] Isaac Charnas,[3] Zoltán Haiman,[1,2,4] John H. Wise[5]
[1]Department of Astronomy, Columbia University, New York, NY 10027, USA
[2]Department of Physics, Columbia University, New York, NY 10027, USA
[3]Columbia Secondary High School, 425 W 123rd Street, New York, NY 10027, USA
[4]Institute of Science and Technology Austria (ISTA), Am Campus 1, Klosterneuburg, Austria
[5]Center for Relativistic Astrophysics, Georgia Institute of Technology, 837 State Street, Atlanta, GA 30332, USA

Accepted XXX. Received YYY; in original form ZZZ

ABSTRACT

Supermassive black holes (SMBHs) with masses $M_\bullet \gtrsim 10^9\,M_\odot$ powering quasars at $z \gtrsim 6$ remain difficult to explain with the growth of stellar-mass seeds. In the 'heavy-seed' scenario, these SMBHs descend from black holes born with masses of $\sim 10^4$–$10^6\,M_\odot$, formed through the collapse of supermassive stars (SMSs) in pristine haloes in which H_2 cooling is suppressed, typically by Lyman–Werner (LW) radiation or by rapid assembly, until the halo reaches the atomic-cooling threshold. Semi-analytic models identify this threshold with a halo virial temperature $T_{\rm act}$, usually 10^4 K, but the predicted abundance of heavy seeds is extremely sensitive to this choice, and the gas inside a halo need not be at its virial temperature. Using cosmological hydrodynamic simulations run with `Enzo` under several LW backgrounds, we measure the gas temperature and the mass inflow rate of every halo above $\sim 10^5\,M_\odot$ between $z = 30$ and $z = 10$, and identify the pristine haloes that never host cold, dense gas. We find that the gas temperature scatters by more than an order of magnitude around $T_{\rm vir}$ at fixed halo mass; that **[MS: X]** per cent of pristine haloes with $T_{\rm vir} \approx 2$–4×10^3 K host gas hotter than 8000 K; and that **[MS: N]** pristine haloes below $T_{\rm vir} = 10^4$ K sustain inflow rates above the $\sim 0.05\,M_\odot\,{\rm yr}^{-1}$ needed to build a SMS. **[MS: One-sentence implication for $T_{\rm act}$ in semi-analytic models.]**

Key words: early Universe – dark ages, reionization, first stars – galaxies: high-redshift – quasars: supermassive black holes – methods: numerical

1 INTRODUCTION

The origin of the supermassive black holes (SMBHs) with masses $\gtrsim 10^9\,M_\odot$ that power quasars at $z \geq 6$ remains poorly understood (Fan et al. 2001, 2003; Mortlock et al. 2011; Wu et al. 2015; Bañados et al. 2018; Yang et al. 2020; Wang et al. 2021). More than 200 such quasars are now known (for recent compilations, see Fan et al. 2023 and Bosman 2022). The *James Webb Space Telescope* has added a population of compact, red, high-redshift sources, the 'Little Red Dots' (LRDs; Kocevski et al. 2023; Harikane et al. 2023; Matthee et al. 2023; Kokorev et al. 2024; Maiolino et al. 2024; Baggen et al. 2024; Guia et al. 2024; Kocevski et al. 2025), thought to host accreting black holes that are overmassive relative to their host galaxies compared to local scaling relations (Pacucci et al. 2023, but see Li et al. 2025). Together, these observations suggest that some early black holes either formed with large masses or grew unusually quickly.

Proposed explanations are usually grouped into 'light' and 'heavy' seed scenarios (Tanaka & Haiman 2009; Volonteri 2010; Johnson & Haardt 2016; Inayoshi et al. 2020; Volonteri et al. 2021; Regan & Volonteri 2024). In the standard picture, primordial gas in dark matter (DM) 'minihaloes' with virial temperatures $T_{\rm vir} < 10^4$ K cools through molecular hydrogen (H_2) and forms Population III (Pop III) stars with masses of $\sim$10–100 $M_\odot$ (Abel et al. 2000; Bromm et al. 2001; Abel et al. 2002; Hirano et al. 2014; Katz et al. 2025), whose remnants are light seeds. If instead H_2 cooling is suppressed until the halo reaches the atomic-cooling limit, cooling by atomic hydrogen drives a nearly isothermal collapse at $T \sim 8000$ K. The resulting high accretion rates, $\dot{M} \gtrsim 0.05\,M_\odot\,{\rm yr}^{-1}$, can build a supermassive star (SMS) of 10^3–$10^5\,M_\odot$ (Hosokawa et al. 2013; Haemmerlé et al. 2018), which collapses into a heavy seed (Loeb & Rasio 1994; Oh & Haiman 2002; Bromm & Loeb 2003; Lodato & Natarajan 2006; Shang et al. 2010; Inayoshi et al. 2014; Regan et al. 2020a). Heavy seeds may also form through hyper-Eddington accretion onto Pop III remnants (Ryu et al. 2016; Inayoshi et al. 2016) or runaway collisions in dense proto-clusters (Boekholt et al. 2018; Tagawa et al. 2020; Escala 2021; Vergara et al. 2022; Schleicher et al. 2022; Pacucci et al. 2025).

Two mechanisms can keep a halo free of H_2 cooling until it reaches the atomic-cooling limit. The first is a strong LW background, which photodissociates H_2 (Haiman et al. 1997; Shang et al. 2010; Visbal et al. 2014; Wolcott-Green et al. 2017). The second is rapid halo as-

★ E-mail: mts2188@columbia.edu

© 2026 The Authors

sembly: when mergers and accretion deepen the potential faster than the gas can cool, compressional and shock heating outpace H_2 cooling and delay collapse (Yoshida et al. 2003; **?**). In the `Renaissance` simulations, Wise et al. (2019) found two haloes in which H_2 cooling did occur, lowering the gas temperature below the atomic-cooling value, yet rapid inflows above the critical SMS rate still reached their cores. Halo assembly history can therefore matter as much as the halo's mass.

Semi-analytic models of heavy-seed formation, which follow halo merger trees rather than gas, must reduce these processes to a criterion on halo properties. Typically, a pristine halo is assumed to form a SMS once its virial temperature, computed from its mass and redshift (e.g. equation 26 of Barkana & Loeb 2001), exceeds a threshold $T_{\rm act}$, usually set to 10^4 K. The predicted heavy-seed abundance depends very strongly on this choice (e.g. Scoggins & Haiman 2024). **?** built Monte Carlo merger trees with estimates of cooling and heating in each halo to identify those that reach the atomic-cooling limit, and computed how often a heavy seed ends up in a dwarf galaxy similar to Leo I. They found that this 'heavy seed survivor' fraction is ∼1 per cent for $T_{\rm act} = 8000$ K, a value motivated by simulations (Regan et al. 2020b), but rises above 50 per cent for lower $T_{\rm act}$. Even modest departures from $T_{\rm act} = 10^4$ K therefore change the predicted number of heavy seeds by orders of magnitude.

The virial temperature describes the depth of the potential well of an idealized, spherically collapsed halo, and roughly corresponds to the temperature of gas in hydrostatic equilibrium within it. The actual gas temperature in a halo of given mass and redshift will scatter around this value, and need not equal it even on average, because of shocks, mergers, ongoing accretion and radiative cooling. How the gas temperature in pristine haloes is distributed around $T_{\rm vir}$, and how this depends on the inflow rate, has not been characterized systematically (but see Shang et al. 2010; Regan et al. 2020b). Kulkarni et al. (2021) carried out an analogous study of the critical mass for Pop III star formation as a function of the LW background, baryon–DM streaming and redshift; here we turn to the atomic-cooling regime.

In this paper we use cosmological hydrodynamic simulations to measure, for every halo above $\sim 10^5$ M$_\odot$ between $z = 30$ and 10, the gas temperature, the mass inflow rate and whether the halo has formed cold, dense gas. We ask three questions. (i) How is $T_{\rm gas}$ distributed around $T_{\rm vir}$ for pristine and star-forming haloes? (ii) What fraction of pristine haloes below $T_{\rm vir} = 10^4$ K contain gas warm enough for atomic cooling? (iii) How often do such haloes sustain inflow rates high enough to form a SMS?

The paper is organized as follows. We describe our simulations and analysis in §2, present our results in §3, discuss their implications and limitations in §4, and summarize in §5.

2 METHODS

2.1 Simulations

We run cosmological hydrodynamic simulations with the adaptive mesh refinement (AMR) code `Enzo` (**?**). `Enzo` follows the DM with an N-body particle-mesh solver and evolves the gas with the piecewise parabolic method on a block-structured AMR grid, which is refined as structures collapse. We follow the non-equilibrium chemistry of primordial gas, including H_2 formation and destruction and the associated radiative cooling, in the presence of a uniform LW background. **[MS: Specify the chemistry network (`Enzo` native or Grackle), whether H_2 self-shielding is included, and the LW spectrum (e.g. $T_\star = 10^5$ K blackbody).]**

Our simulations use a cubic box of comoving side length $L = 2\,h^{-1}$ Mpc with a 512^3 root grid and 512^3 DM particles, giving a DM particle mass of $\approx 6.7\times10^3$ M$_\odot$. **[MS: The earlier draft quoted $4\,h^{-1}$ Mpc with 1024^3 particles. The particle mass and cell size are identical in the two configurations; confirm which box was used for the runs analysed here.]** We allow up to four levels of refinement (refinement factor 2), so the finest cells are $L/(512\times2^4) \approx 0.24\,h^{-1}$ kpc comoving, or ≈17 pc and ≈33 pc physical at $z = 20$ and $z = 10$, respectively. Cells are refined when their baryon or DM mass exceeds **[MS: N]** times the corresponding mass of a root-grid cell **[MS: and/or when the Jeans length is resolved by fewer than N cells; confirm]**. We run three otherwise identical simulations with uniform LW backgrounds of $J_{\rm LW} = 1$, 10 and 100, in units of 10^{-21} erg s^{-1} cm^{-2} Hz^{-1} sr^{-1}. Each is started at $z =$ **[MS : Z]** **[MS: (IC generator)]**, and we write outputs at $z = 30, 27, 25, 24, \ldots, 10$, in steps of $\Delta z = 1$ below $z = 25$.

We adopt a flat ΛCDM cosmology with $\Omega_{\rm m} = 0.32$, $\Omega_\Lambda = 0.68$, $\Omega_{\rm b} = 0.049$, $h = 0.67$ and $\sigma_8 = 0.81$, consistent with Planck Collaboration et al. (2020). **[MS: The earlier draft listed $\Omega_{\rm m} = 0.307$, $\Omega_{\rm b} = 0.0486$ (closer to Planck 2015); the analysis script assumes $\Omega_{\rm m} = 0.32$, $\Omega_{\rm b} = 0.049$. Use the values in the `Enzo` parameter file and make the analysis match.]**

We identify DM haloes with the Rockstar phase-space halo finder (Behroozi et al. 2012a) and link them across outputs into merger trees with consistent-trees (Behroozi et al. 2012b). Halo catalogues and trees are read with `ytree` (**?**), and the simulation outputs are analysed with `yt` (**?**). We use the Rockstar virial mass $M_{\rm vir}$ and radius $r_{\rm vir}$ throughout, defined with the overdensity of **?**, and only consider haloes with $M_{\rm vir} > 10^5$ M$_\odot$ ($\gtrsim$15 DM particles). Lower-mass haloes are kept in the merger trees for bookkeeping only. **[MS: The earlier draft used 5×10^4 M$_\odot$; the current analysis uses 10^5 M$_\odot$ in the trees and 2×10^5 M$_\odot$ for the gas measurements in the final outputs. Choose one and state it.]**

2.2 Virial temperature

We assign each halo a virial temperature following equation (26) of Barkana & Loeb (2001),

$$T_{\rm vir} = 1.98\times10^4\,{\rm K}\left(\frac{\mu}{0.6}\right)\left(\frac{M_{\rm vir}}{10^8\,h^{-1}\,{\rm M}_\odot}\right)^{2/3} \times\left[\frac{\Omega_{\rm m}}{\Omega_{\rm m}^z}\,\frac{\Delta_{\rm c}}{18\pi^2}\right]^{1/3}\left(\frac{1+z}{10}\right), \tag{1}$$

where $\Omega_{\rm m}^z$ is the matter density parameter at redshift z, $\Delta_{\rm c} = 18\pi^2 + 82d - 39d^2$ with $d = \Omega_{\rm m}^z - 1$ (**?**), and $\mu = 1.22$ is the mean molecular weight of neutral primordial gas. This is the quantity that semi-analytic models compare against $T_{\rm act}$, so we use it as our reference temperature throughout.

2.3 Gas properties

For each halo we select the gas cells within a sphere of radius $r_{\rm vir}$ centred on the Rockstar halo centre, using the finest available cell at each location. From these cells we compute the following quantities.

- **Mean gas temperature**, $T_{\rm gas}$: the mass-weighted mean temperature of all gas within $r_{\rm vir}$.
- **Warm-gas fraction**, $f_{\rm warm}$: the fraction of the gas mass within $r_{\rm vir}$ with $T > 8000$ K.
- **Dense-gas temperature**, $T_{\rm dense}$: the mass-weighted temperature of gas with $n_{\rm H} > 10\,{\rm cm}^{-3}$.

• **Core temperature**, $T_{\rm core}$: the mass-weighted temperature within $0.1\,r_{\rm vir}$ of the gas density maximum.

[MS: State which of these is plotted as $T_{\rm gas}$ in each figure. The current figures appear to use the mass-weighted mean within $r_{\rm vir}$.]

The mean temperature $T_{\rm gas}$ is the quantity most directly comparable to $T_{\rm vir}$. However, it mixes shock-heated, diffuse gas in the halo outskirts with the dense gas that will actually collapse, so we also record $T_{\rm dense}$, $T_{\rm core}$ and $f_{\rm warm}$, which track whether the collapsing gas is on the atomic-cooling ($T \approx 8000\,{\rm K}$) or H_2-cooling ($T \sim 200\,{\rm K}$) track.

2.4 Mass inflow rates

We measure the mass flux through spherical shells in the rest frame of the halo, subtracting the Rockstar bulk velocity of the halo, $\mathbf{v}_{\rm h}$, from each cell's velocity before projecting onto the radial direction. For a shell $r_{\rm in} \le r < r_{\rm out}$,

$$\dot{M} = \frac{1}{r_{\rm out} - r_{\rm in}} \sum_{i\,\in\,{\rm shell}} m_i\,(\mathbf{v}_i - \mathbf{v}_{\rm h}) \cdot \hat{\mathbf{r}}_i, \qquad (2)$$

where m_i and $\mathbf{v}_i$ are the gas mass and velocity of cell i, and $\hat{\mathbf{r}}_i$ is the unit vector from the shell centre to the cell. Negative values indicate inflow; we quote inflow rates as positive numbers below. We evaluate equation (2) in three shells:

(i) an outer shell, 0.5–1 $r_{\rm vir}$ about the halo centre, which measures the supply of gas onto the halo;
(ii) an inner shell, 0.05–0.15 $r_{\rm vir}$ about the gas density maximum, which measures the supply to the core;
(iii) a shell 3–5 finest cells from the gas density maximum, the smallest radius at which the flux is resolved.

For each shell we also record the number of cells and their median size, so that unresolved measurements can be excluded. At our resolution the outer shell is resolved by $\gtrsim$4 cells for $M_{\rm vir} \gtrsim 10^6\,{\rm M}_\odot$, while the inner shell is resolved only for $M_{\rm vir} \gtrsim$ a few $\times 10^7\,{\rm M}_\odot$. Unless stated otherwise, inflow rates refer to the outer shell. **[MS: Confirm which shell the figures use.]**

We compare these rates with the critical rate for SMS formation, $\dot{M}_{\rm crit} \approx 0.05\,{\rm M}_\odot\,{\rm yr}^{-1}$ (Hosokawa et al. 2013; Haemmerlé et al. 2018). Because $\dot{M}$ grows steeply with halo mass ($\langle\dot{M}\rangle \propto M^{1.1}$; **?**), we also consider the specific inflow rate $\dot{M}/M_{\rm vir}$ when looking for the effect of inflow on the gas temperature at fixed mass.

2.5 Star-forming and pristine haloes

Following Kulkarni et al. (2021), building on **?**, we label a halo as star-forming if it contains at least one cell in which the gas is both cold and dense,

$$T < 0.5\,T_{\rm vir} \quad \text{and} \quad n_{\rm H} > 100\,{\rm cm}^{-3}, \qquad (3)$$

within $2\,r_{\rm vir}$ of the halo centre. Both conditions must hold in the same cell. Requiring them separately, anywhere in the halo's surroundings, is satisfied almost trivially, because the unshocked intergalactic and infalling gas at these redshifts is at $T \sim$ 10–100 K, well below $0.5\,T_{\rm vir}$. We call a halo pristine if neither it nor any of its progenitors in the merger tree has ever satisfied equation (3).

Kulkarni et al. (2021) applied equation (3) in simulations with $\sim$1 pc resolution at $z = 20$, in which the Jeans length is resolved by at least four cells (**?**). At our $\sim$17–33 pc resolution, the Jeans length of gas at $T = 200\,{\rm K}$ and $n_{\rm H} = 100\,{\rm cm}^{-3}$ ($\approx$17 pc) is comparable to a single cell, so collapsing cold gas may never reach the density threshold in our runs. This biases the classification towards 'pristine'. **[MS: Describe how we address this: e.g. (a) recalibrate the density threshold, or add a core H_2-fraction criterion with $x_{\rm H_2} \gtrsim 10^{-4}$–$10^{-3}$ (?), using matched lower- and higher-resolution runs of the same initial conditions; or (b) re-simulate pristine candidates at higher resolution. Report the fraction of haloes whose classification changes.]**

3 RESULTS

3.1 Gas temperature versus virial temperature

Fig. 1 shows the median ratio $T_{\rm gas}/T_{\rm vir}$ as a function of halo mass and redshift, for pristine (left) and star-forming (right) haloes. In both populations the gas in low-mass haloes ($M \lesssim 10^6\,{\rm M}_\odot$) is hotter than $T_{\rm vir}$. In these haloes, accretion shocks and adiabatic compression heat the gas to temperatures that the shallow potential cannot contain in equilibrium. The ratio decreases with mass. Star-forming haloes fall well below unity above $M \sim 10^{6.5}\,{\rm M}_\odot$, as expected for haloes in which gas has cooled, whereas pristine haloes remain within a factor of a few of $T_{\rm vir}$ up to the atomic-cooling mass. Pristine haloes are rare above the $T_{\rm vir} = 10^4$ K line (solid curve), and almost all haloes above it have formed cold, dense gas.

Fig. 2 shows the distribution of $\log_{10}(T_{\rm gas}/T_{\rm vir})$ in four mass bins at $z = 10$, 12 and 14. Each histogram is normalized separately, so the panels compare the shapes of the distributions, not the number of haloes. In every mass bin the distribution is broad, spanning more than an order of magnitude. For star-forming haloes it extends to $T_{\rm gas}/T_{\rm vir} \sim 0.1$, reflecting cooled gas, whereas for pristine haloes it is concentrated at $T_{\rm gas} \gtrsim T_{\rm vir}$. The distributions shift to higher $T_{\rm gas}/T_{\rm vir}$ towards lower redshift. **[MS: Interpret this redshift trend, e.g. higher accretion-shock temperatures as haloes grow, or the evolution of the LW-suppressed population.]**

Fig. 3 shows the median and 16th–84th percentile range of $T_{\rm gas}/T_{\rm vir}$ as a function of $T_{\rm vir}$. The median ratio decreases from $\approx$0.5 at $T_{\rm vir} =$ 2000 K to $\approx$0.1 at $T_{\rm vir} = 10^4$ K, so on average the gas in more massive haloes lies further below its virial temperature. The maximum ratio in each bin, however, exceeds the ratio needed for $T_{\rm gas} = 8000$ or 10^4 K (green and orange curves) for $T_{\rm vir} \lesssim$7000 K. Some haloes far below the nominal threshold therefore contain gas that is, on average, hot enough for atomic cooling. **[MS: Specify whether this figure includes all haloes or only pristine haloes.]**

3.2 Warm gas in pristine haloes below the atomic-cooling threshold

To quantify how common such haloes are, Fig. 4 shows the fraction of pristine haloes in each $T_{\rm vir}$ bin whose gas temperature exceeds $T_{\rm thr} = 7000$, 8000, 9000 and 10^4 K. The fraction with $T_{\rm gas} > 8000$ K peaks at $\approx$25 per cent for $T_{\rm vir} \approx 2$–3×10^3 K, and remains at $\sim$5–20 per cent up to $T_{\rm vir} \approx 7000$ K. Gas temperatures above 10^4 K are rarer, at $\lesssim$6 per cent in all bins. Because Lyman-α cooling quickly brings gas above $\sim 10^4$ K back to $\approx$8000 K, temperatures well above this value are likely transient, shock-heated gas rather than a long-lived atomic-cooling core. **[MS: Check with $T_{\rm dense}$ and $f_{\rm warm}$ whether the warm gas in these haloes is dense, central gas or diffuse, shocked gas.]**

3.3 Mass inflow rates

Fig. 5 shows $T_{\rm gas}/T_{\rm vir}$ as a function of the mass inflow rate for all haloes between $z = 10$ and 18. Most haloes have $\dot{M} \sim 10^{-5}$–$10^{-2}\,{\rm M}_\odot\,{\rm yr}^{-1}$, and a tail extends above $0.1\,{\rm M}_\odot\,{\rm yr}^{-1}$. Haloes with higher inflow rates lie more often above $T_{\rm gas} = T_{\rm vir}$. Part of this trend is expected from mass alone, since both $\dot{M}$ and $T_{\rm gas}/T_{\rm vir}$ correlate with halo mass, so we will test it at fixed mass using $\dot{M}/M_{\rm vir}$ (§2.4). **[MS: Add this fixed-mass comparison, ideally separately for each $J_{\rm LW}$; dynamical heating predicts warmer cores at higher specific inflow (Yoshida et al. 2003; ?).]**

Fig. 6 shows the cumulative number of haloes with inflow rates above $\dot{M}_{\rm thr} = 0.05$, 0.10 and $0.15\,{\rm M}_\odot\,{\rm yr}^{-1}$, as a function of gas temperature, for star-forming and pristine haloes. About 90 pristine haloes exceed the nominal critical rate of $0.05\,{\rm M}_\odot\,{\rm yr}^{-1}$, and ≈40 exceed $0.15\,{\rm M}_\odot\,{\rm yr}^{-1}$. Many of these have $T_{\rm gas} \lesssim 5000\,{\rm K}$, well below the atomic-cooling temperature. These haloes are candidates for SMS formation driven by inflow rather than by reaching $T_{\rm vir} = 10^4$ K, as found by Wise et al. (2019). **[MS: Give their $T_{\rm vir}$ distribution, LW dependence, and whether the inner-shell inflow (where resolved) is also high.]**

4 DISCUSSION

4.1 Implications for semi-analytic models

[MS: Translate the results into a prescription for semi-analytic models. Options: (i) a probability $P(T_{\rm gas} > 8000\,{\rm K} \,|\, T_{\rm vir}, z)$ to replace the step function at $T_{\rm act}$; (ii) an effective $T_{\rm act}$ as a function of $J_{\rm LW}$ and z; (iii) an inflow-based criterion using $\dot{M}/M$. Quantify how adopting it changes the heavy-seed survivor fraction of ?.]

4.2 Comparison with previous work

[MS: Compare with Regan et al. (2020b) (star-free atomic-cooling haloes in `Renaissance`), Wise et al. (2019) (rapidly growing haloes), Kulkarni et al. (2021) and Schauer et al. (2021) (Pop III critical mass), and the selection criteria of McCaffrey et al. (2025).]

4.3 Limitations

Our results are subject to the following limitations.

- **Resolution.** With four levels of refinement, our finest cells are ∼20–30 pc. We do not resolve the cores of minihaloes, which affects the star-forming classification (§2.5), $T_{\rm core}$, and the inner-shell inflow rates of haloes below $\sim 10^7\,{\rm M}_\odot$.
- **Halo statistics at low mass.** Haloes near our mass cut contain only ∼15–30 DM particles, so their merger-tree links and virial quantities are noisy.
- **Physics not included.** **[MS: e.g. baryon–DM streaming velocities, X-ray background, local (non-uniform) LW sources, and metal enrichment from neighbouring star-forming haloes.]**

5 CONCLUSIONS

We have measured the gas temperatures and mass inflow rates of haloes between $z = 30$ and 10 in cosmological simulations with LW backgrounds of $J_{\rm LW} = 1$, 10 and 100, and compared them with the virial temperatures used in semi-analytic models of heavy-seed formation. Our main findings are:

(i) At fixed halo mass and redshift, the mean gas temperature scatters around $T_{\rm vir}$ by more than an order of magnitude. In pristine haloes it typically exceeds $T_{\rm vir}$ below $\sim 10^6\,{\rm M}_\odot$ and approaches $T_{\rm vir}$ near the atomic-cooling mass.

(ii) A significant fraction of pristine haloes below the canonical threshold, up to ∼25 per cent at $T_{\rm vir} \approx 2$–3×10^3 K, contain gas with $T_{\rm gas} > 8000$ K.

(iii) **[MS: N]** pristine haloes sustain inflow rates above the critical SMS rate of $\sim 0.05\,{\rm M}_\odot\,{\rm yr}^{-1}$ while having $T_{\rm vir} < 10^4$ K.

(iv) **[MS: Result on the dependence on $J_{\rm LW}$.]**

[MS: Closing statement on what this implies for $T_{\rm act}$ and the abundance of heavy seeds.]

ACKNOWLEDGEMENTS

[MS: Update grant numbers.] ZH acknowledges support from NSF grant AST-2006176. Simulations and analysis were performed with NSF ACCESS allocations AST-120046 and AST-140041 on the Stampede3 resource at the Texas Advanced Computing Center. This work made use of `yt` (**?**), `ytree` (**?**) and `matplotlib` (Hunter 2007).

DATA AVAILABILITY

The code used to analyse the simulations and produce the figures in this paper is available at `https://github.com/mscoggs/ACH_properties`. The simulation data will be shared on reasonable request to the corresponding author.

REFERENCES

Abel T., Bryan G. L., Norman M. L., 2000, ApJ, 540, 39
Abel T., Bryan G. L., Norman M. L., 2002, Science, 295, 93
Bañados E., et al., 2018, Nature, 553, 473
Baggen J. F. W., et al., 2024, ApJ, 977, L13
Barkana R., Loeb A., 2001, Phys. Rep., 349, 125
Behroozi P. S., Wechsler R. H., Wu H.-Y., Busha M. T., Klypin A. A., Primack J. R., 2012b, Consistent Trees: Gravitationally Consistent Halo Catalogs and Merger Trees for Precision Cosmology, Astrophysics Source Code Library, record ascl:1210.011 (ascl:1210.011)
Behroozi P., Wechsler R., Wu H.-Y., 2012a, Rockstar: Phase-space halo finder, Astrophysics Source Code Library, record ascl:1210.008 (ascl:1210.008)
Boekholt T. C. N., Schleicher D. R. G., Fellhauer M., Klessen R. S., Reinoso B., Stutz A. M., Haemmerlé L., 2018, MNRAS, 476, 366
Bosman S. E. I., 2022, Zenodo
Bromm V., Loeb A., 2003, ApJ, 596, 34
Bromm V., Ferrara A., Coppi P., Larson R., 2001, MNRAS, 328, 969
Escala A., 2021, ApJ, 908, 57
Fan X., et al., 2001, The Astronomical Journal, 122, 2833
Fan X., et al., 2003, The Astronomical Journal, 125, 1649
Fan X., Bañados E., Simcoe R. A., 2023, ARAA, 61, 373
Guia C. A., Pacucci F., Kocevski D. D., 2024, Research Notes of the American Astronomical Society, 8, 207
Haemmerlé L., Woods T. E., Klessen R. S., Heger A., Whalen D. J., 2018, MNRAS, 474, 2757
Haiman Z., Rees M. J., Loeb A., 1997, ApJ, 476, 458
Harikane Y., et al., 2023, arXiv e-prints, p. arXiv:2303.11946
Hirano S., Hosokawa T., Yoshida N., Umeda H., Omukai K., Chiaki G., Yorke H. W., 2014, ApJ, 781, 60
Hosokawa T., Yorke H. W., Inayoshi K., Omukai K., Yoshida N., 2013, ApJ, 778, 178
Hunter J. D., 2007, Computing in Science & Engineering, 9, 90
Inayoshi K., Omukai K., Tasker E., 2014, MNRAS, 445, L109

Inayoshi K., Haiman Z., Ostriker J. P., 2016, MNRAS, 459, 3738
Inayoshi K., Visbal E., Haiman Z., 2020, Annual Review of Astronomy and Astrophysics, 58, 27
Johnson J. L., Haardt F., 2016, Publ. Astron. Soc. Australia, 33, e007
Katz O. Z., Redigolo D., Volansky T., 2025, J. Cosmology Astropart. Phys., 2025, 047
Kocevski D. D., et al., 2023, ApJ, 954, L4
Kocevski D. D., et al., 2025, ApJ, 986, 126
Kokorev V., et al., 2024, ApJ, 968, 38
Kulkarni M., Visbal E., Bryan G. L., 2021, ApJ, 917, 40
Li J., et al., 2025, ApJ, 981, 19
Lodato G., Natarajan P., 2006, MNRAS, 371, 1813
Loeb A., Rasio F. A., 1994, ApJ, 432, 52
Maiolino R., et al., 2024, A&A, 691, A145
Matthee J., et al., 2023, arXiv e-prints, p. arXiv:2306.05448
McCaffrey J., Regan J., Smith B., Wise J., O'Shea B., Norman M., 2025, The Open Journal of Astrophysics, 8, 11
Mortlock D. J., et al., 2011, Nature, 474, 616
Oh S. P., Haiman Z., 2002, ApJ, 569, 558
Pacucci F., Nguyen B., Carniani S., Maiolino R., Fan X., 2023, ApJ, 957, L3
Pacucci F., Hernquist L., Fujii M., 2025, arXiv e-prints, p. arXiv:2509.02664
Planck Collaboration et al., 2020, A&A, 641, A6
Regan J., Volonteri M., 2024, The Open Journal of Astrophysics, 7, 72
Regan J. A., Haiman Z., Wise J. H., O'Shea B. W., Norman M. L., 2020a, The Open Journal of Astrophysics, 3
Regan J. A., Wise J. H., O'Shea B. W., Norman M. L., 2020b, MNRAS, 492, 3021
Ryu T., Tanaka T. L., Perna R., Haiman Z., 2016, MNRAS, 460, 4122
Schauer A. T. P., Glover S. C. O., Klessen R. S., Clark P., 2021, MNRAS, 507, 1775
Schleicher D. R. G., et al., 2022, MNRAS, 512, 6192
Scoggins M. T., Haiman Z., 2024, MNRAS, 531, 4584
Shang C., Bryan G. L., Haiman Z., 2010, MNRAS, 402, 1249
Tagawa H., Haiman Z., Kocsis B., 2020, ApJ, 892, 36
Tanaka T., Haiman Z., 2009, ApJ, 696, 1798
Vergara M. C., Escala A., Schleicher D. R. G., Reinoso B., 2022, Global instability by runaway collisions in nuclear stellar clusters: Numerical tests of a route for massive black hole formation, doi:10.48550/ARXIV.2209.15066, https://arxiv.org/abs/2209.15066
Visbal E., Haiman Z., Bryan G. L., 2014, MNRAS: Letters, 442, L100
Volonteri M., 2010, The Astronomy and Astrophysics Review, 18, 279
Volonteri M., Habouzit M., Colpi M., 2021, Nature Reviews Physics, 3, 732
Wang F., et al., 2021, ApJ, 908, 53
Wise J. H., Regan J. A., O'Shea B. W., Norman M. L., Downes T. P., Xu H., 2019, Nature, 566, 85
Wolcott-Green J., Haiman Z., Bryan G. L., 2017, MNRAS, 469, 3329
Wu X.-B., et al., 2015, Nature, 518, 512
Yang X., et al., 2020, ApJ, 904, 200
Yoshida N., Abel T., Hernquist L., Sugiyama N., 2003, ApJ, 592, 645

This paper has been typeset from a TEX/LATEX file prepared by the author.

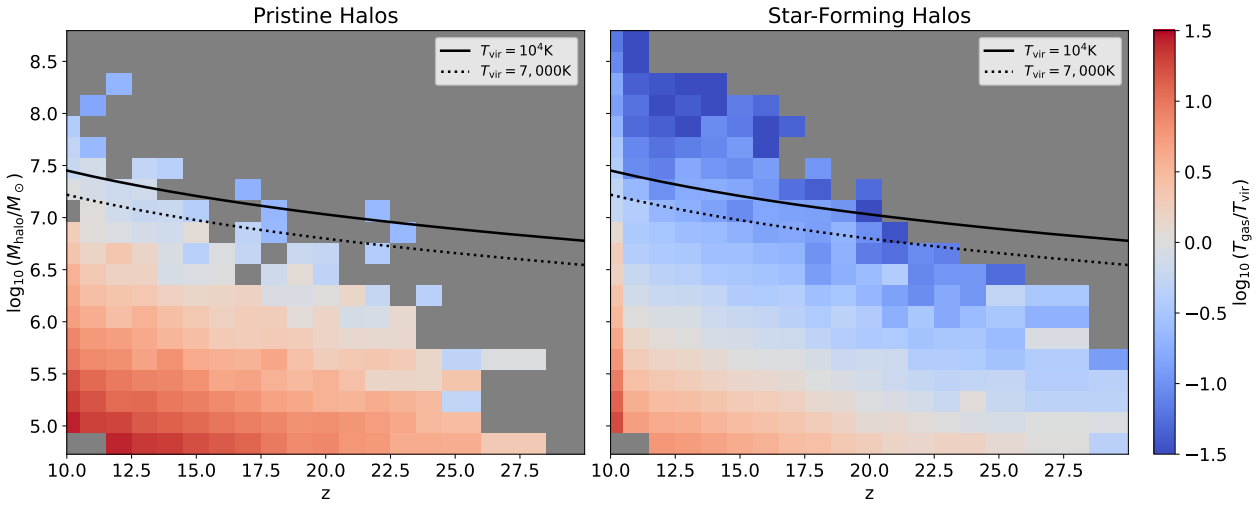


Figure 1. Median $\log_{10}(T_{\rm gas}/T_{\rm vir})$ in bins of halo mass and redshift, for pristine haloes (left) and star-forming haloes (right). Grey bins contain no haloes. The solid and dotted black curves show the masses corresponding to $T_{\rm vir} = 10^4$ K and 7000 K (equation 1). Gas in low-mass haloes is hotter than $T_{\rm vir}$ in both populations; above $\sim 10^{6.5}$ M$_\odot$, star-forming haloes have $T_{\rm gas} \ll T_{\rm vir}$, while the few pristine haloes remain within a factor of a few of $T_{\rm vir}$.

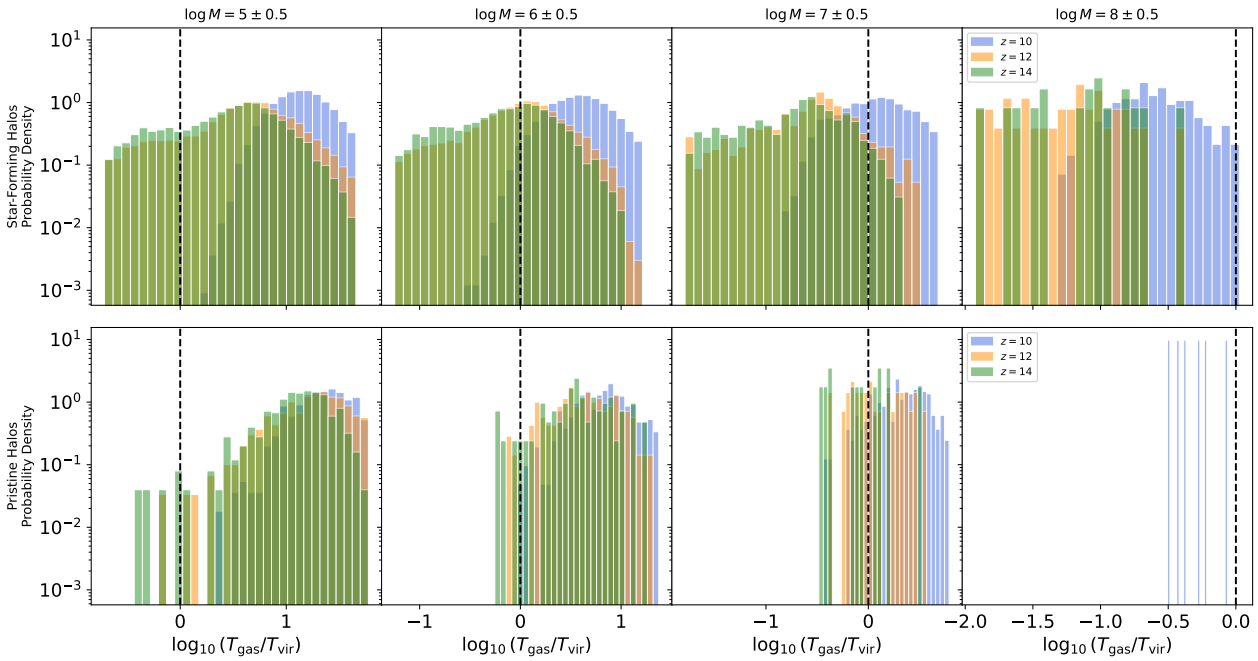


Figure 2. Normalized distributions of $\log_{10}(T_{\rm gas}/T_{\rm vir})$ for star-forming (top) and pristine (bottom) haloes, in four bins of $\log_{10}(M/{\rm M}_\odot)$ (columns) at $z = 10$, 12 and 14 (colours). The dashed line marks $T_{\rm gas} = T_{\rm vir}$. Each histogram is normalized individually, so the panels compare shapes rather than numbers of haloes. Pristine haloes are concentrated at $T_{\rm gas} \gtrsim T_{\rm vir}$, whereas star-forming haloes extend to $T_{\rm gas}/T_{\rm vir} \sim 0.1$. **[MS: The $\log M = 8$ pristine panel contains only a handful of haloes; consider dropping it or labelling the counts.]**

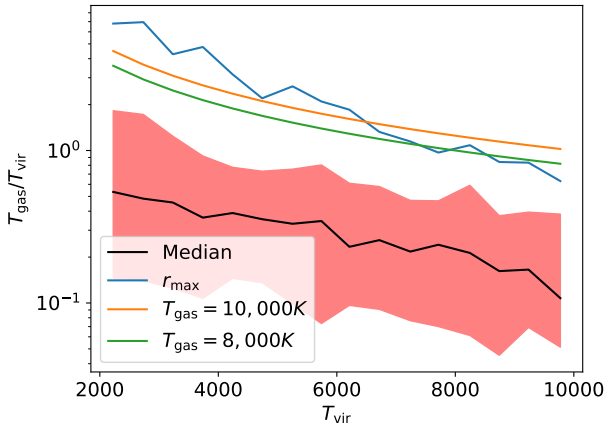


Figure 3. T_{gas}/T_{vir} as a function of T_{vir}. The black line shows the median in each bin and the red band the 16th–84th percentile range; the blue line (r_{max}) shows the maximum ratio in each bin. The orange and green curves show the ratio corresponding to $T_{gas} = 10^4$ K and 8000 K. The median ratio falls with increasing T_{vir}, but the most extreme haloes in each bin reach $T_{gas} \geq 8000$ K for $T_{vir} \lesssim 7000$ K.

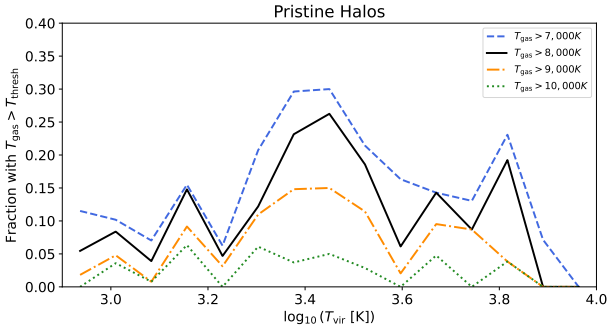


Figure 4. Fraction of pristine haloes in each T_{vir} bin whose gas temperature exceeds $T_{thr} = 7000$ K (dashed blue), 8000 K (solid black), 9000 K (dash-dotted orange) and 10^4 K (dotted green). Up to ≈25 per cent of pristine haloes with $T_{vir} \approx 2$–3×10^3 K contain gas hotter than 8000 K.

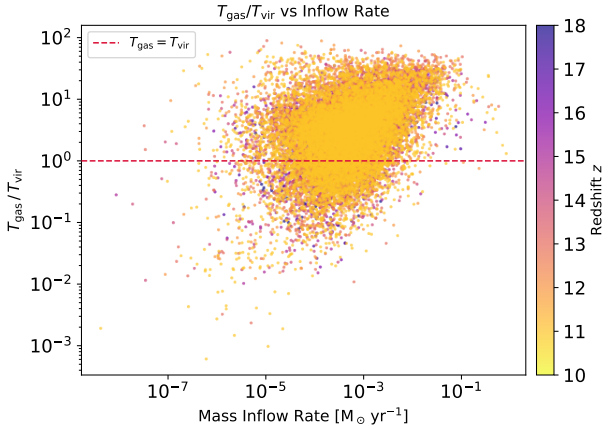


Figure 5. T_{gas}/T_{vir} against the mass inflow rate through the outer shell (0.5–1 r_{vir}), for all haloes at $z = 10$–18, coloured by redshift. The dashed red line marks $T_{gas} = T_{vir}$. Haloes with higher inflow rates are more often hotter than their virial temperature; part of this trend reflects the correlation of both quantities with halo mass (see text).

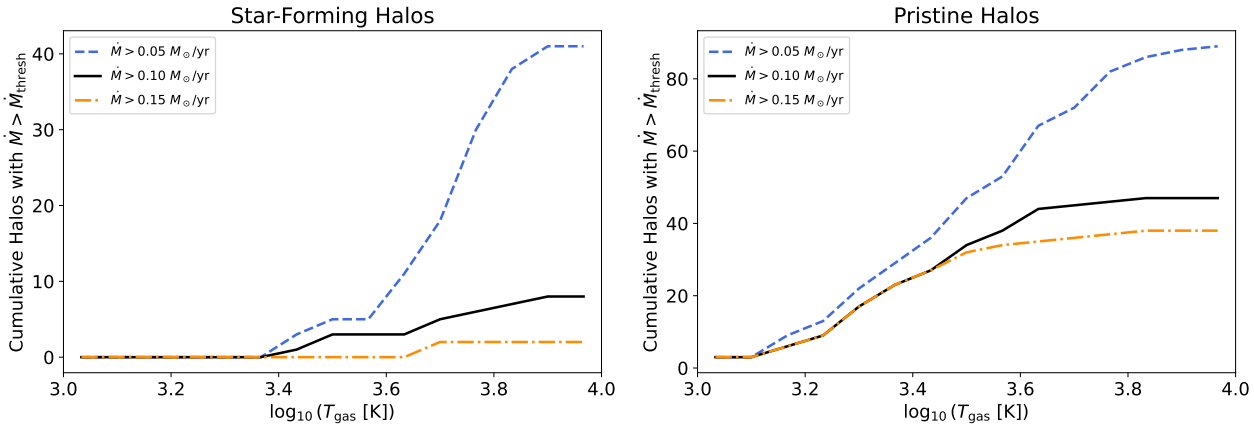


Figure 6. Cumulative number of star-forming (left) and pristine (right) haloes with inflow rates above $\dot{M}_{\rm thr}$ = 0.05 (dashed blue), 0.10 (solid black) and 0.15 $\mathrm{M_\odot\ yr^{-1}}$ (dash-dotted orange), as a function of gas temperature. Many pristine haloes exceed the critical rate for SMS formation while their gas is well below the atomic-cooling temperature.